The Influence of d^{10}-d^{10} Interactions in $Ag_5Te_{1.8}Se_{0.2}Cl$ and $Ag_5Te_{1.6}Se_{0.4}Cl$ on Structural and Thermoelectric Properties

Nadine Eckstein[a], Jean-Louis Bobet[b], Bernard Chevalier[b], and Tom Nilges[a]

[a] Department Chemie, Technische Universität München, Lichtenbergstraße 4, 85747 Garching, Germany
[b] CNRS, Université de Bordeaux, ICMCB, Avenue du Docteur A. Schweitzer 87, 33608 PESSAC cedex, France

Reprint requests to Prof. Dr. Tom Nilges. Fax: +49(0)89-289-13762. E-mail: tom.nilges@lrz.tum.de

Z. Naturforsch. **2011**, *66b,* 1005 – 1014; received August 1, 2011

Measurements of the thermopower and of the thermal diffusivity and a detailed analysis of the structural features by temperature-dependent single-crystal structure determinations of silver ion-conducting $Ag_5Te_{1.8}Se_{0.2}Cl$ and $Ag_5Te_{1.6}Se_{0.4}Cl$ were performed to investigate the interaction of silver ions in their disordered state. The substituted phases show an order/disorder phase transition at 273.3(2) and 302.5(2) K, respectively, accompanied by a drop of the thermal diffusivity and a minimum plateau of the thermopower right after the transition. Silver ions are arranged in well-defined strands along the crystallographic *c* axis characterized by a set of not fully occupied sites. $Ag_5Te_{1.6}Se_{0.4}Cl$ shows a negative thermal expansion during temperature rise right after the silver order/disorder phase transition; this is explicable by attractive d^{10}-d^{10} interactions within the disordered silver substructure. After the minimum values of the thermopower have been reached, these values rise in parallel to the decrease of the d^{10}-d^{10} interactions. $Ag_5Te_{1.6}Se_{0.4}Cl$ shows a very low value of the thermal diffusivity of 0.070 $mm^2\ s^{-1}$ at 300.7 K.

Key words: Silver, Tellurium, Polytelluride, Thermoelectrics, d^{10}-d^{10} Interactions

Introduction

One of the most important problems to be solved in our society is an efficient energy conversion and storage [1, 2]. Thermoelectrics can deliver a significant contribution to this problem but they need to be improved and further developed [3]. Recently, a new concept for the improvement of thermopower has been proposed connecting thermoelectricity and modulation of the electronic structure of compounds by the generation or the use of low-dimensional attractive interactions in solids [4, 5]. Such a concept was found for Peierls-distorted polyanionic Te and polycationic In chains in the coinage metal polychalcogenide halide $Ag_{10}Te_4Br_3$ [5, 6], and in $In_4Se_{3-\delta}$ [4]. The Te chains in $Ag_{10}Te_4Br_3$ lead to a modulation of the electronic structure, resulting in a pnp-switch of the semiconducting properties and a huge drop of thermopower of about 1400 $\mu V\,K^{-1}$ during a structural phase transition. The effective modulation is possible because the silver ion mobility, a common feature for silver halide containing chalcogenides like the title compound or compounds containing complex oxo anions like Ag_3ITeO_4, $Ag_4I_2SeO_4$, $Ag_9I_3(SeO_4)_2(IO_3)_2$, and $Ag_8I_2(CrO_4)_3$ [7 – 9], is effectively optimized. On the other hand, heavy chalcogenides (Se or Te) are excellent candidates for modulations due to their pronounced tendency to form primary and secondary attractive interactions [10].

Recently, the occurrence of attractive d^{10}-d^{10} interactions has been proved by a thermoelectric characterization of Ag_5Te_2Cl in its silver ion disordered high-temperature α-polymorph. Significant variations of the thermoelectric properties like thermopower, thermal diffusivity and the thermoelectric *figure of merit* can be assigned to such oriented, low-dimensional interactions around the silver order/disorder phase transition [11, 12].

Herein we will analyze the influence of the partial substitution of tellurium in Ag_5Te_2Cl by selenium on the thermoelectric performance of this class of compounds.

Results and Discussion

Trimorphic $Ag_5Te_{1.8}Se_{0.2}Cl$ and $Ag_5Te_{1.6}Se_{0.4}Cl$ are substituted phases of Ag_5Te_2Cl showing re-

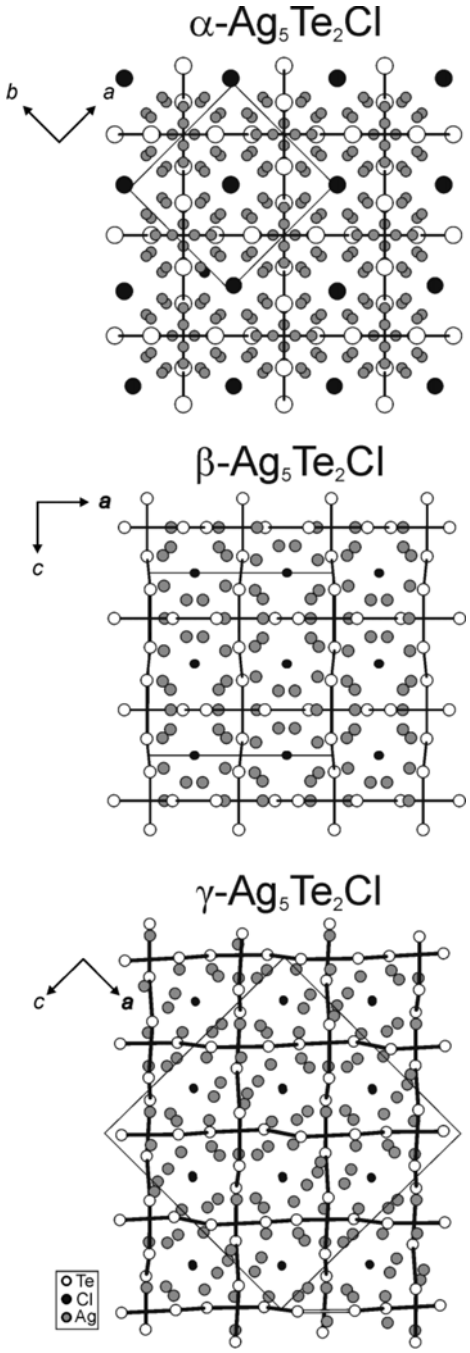

Fig. 1. Structure sections of the α-, β- and γ-Ag_5Te_2Cl structure type (structural data are taken from ref. [14]).

versible order/disorder transitions (β-α) at 303(1) and 273(1) K, respectively [11]. In Fig. 1 a representative structure projection is given for each polymorph, and in Fig. 2 the silver distribution is denoted

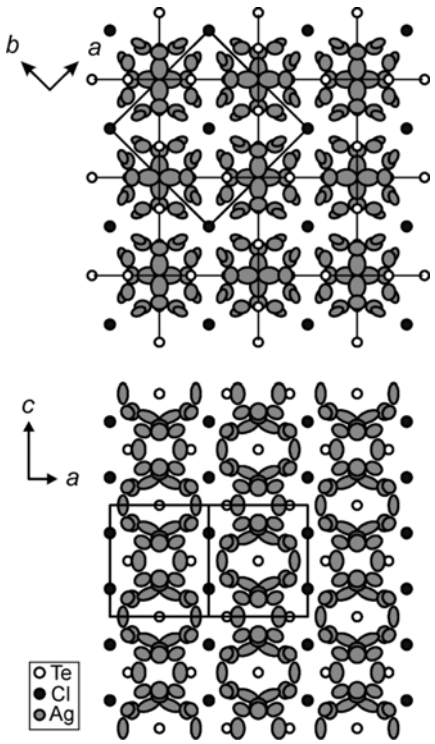

Fig. 2. Crystal structure sections of α-Ag_5Te_2Cl (573 K). The silver ions are forming a strand of delocalized silver along the *c* axis. Displacement parameters are shown at the 50 % level.

for the α-Ag_5Te_2Cl polymorph. $Ag_5Te_{1.8}Se_{0.2}Cl$ and $Ag_5Te_{1.6}Se_{0.4}Cl$ were prepared by literature procedures [12] and characterized by powder phase X-ray analyses and EDX measurements [13]. Phase-pure samples were used to verify the polymorphism of these compounds; effects observed in the differential scanning calorimetry measurements (DSC) are equal to the literature values [15] and lie at the onset temperatures of 273(1) and 303(1) K, respectively [12]. The endothermic effect representing the β-α phase transition is shifted to a lower temperature compared with the ternary phase. The temperature shift can be addressed by the grade of substitution and by the choice of the elements [13, 15, 16]. Systematic investigations of physical properties were started right after the mentioned phase transition.

The thermopower measurements of $Ag_5Te_{1.8}Se_{0.2}Cl$ and $Ag_5Te_{1.6}Se_{0.4}Cl$ show minimum values at the low end of the applied temperature range around 300 K in both cases (Fig. 3). A thermopower minimum plateau for $Ag_5Te_{1.8}Se_{0.2}Cl$ emerges right after the order/disorder phase transition, and thereafter the value

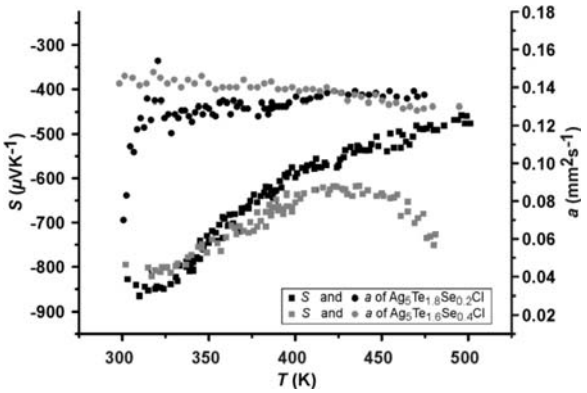

Fig. 3. Measured thermopower S in $\mu V\,K^{-1}$ (left axis) and thermal diffusivity a in $mm^2\,s^{-1}$ (right axis) in the temperature range of 300 – 500 K. The minimum of the thermal diffusivity is near the β-α phase transition of $Ag_5Te_{1.8}Se_{0.2}Cl$ and $Ag_5Te_{1.6}Se_{0.4}Cl$. The minimal value of the measurement is 0.070 $mm^2\,s^{-1}$ at 300.7 K for $Ag_5Te_{1.6}Se_{0.4}Cl$ in the thermopower range from -468 to -889 $\mu V\,K^{-1}$. Consequently the full thermopower effect is located near the order/disorder phase transition and rises to a maximum value of -468 $\mu V\,K^{-1}$ at 492 K.

rises in an analogous way as the thermopower of Ag_5Te_2Cl (Fig. 3). A comparable but less pronounced effect can be observed in the case of $Ag_5Te_{1.6}Se_{0.4}Cl$. Compared with the thermopower plateau in Ag_5Te_2Cl, which is deeper and more pronounced, the substitution obviously reduces the modulation effect drastically.

The thermal diffusivity of $Ag_5Te_{1.8}Se_{0.2}Cl$ and $Ag_5Te_{1.6}Se_{0.4}Cl$ was determined in the range between 0.12 and 0.14 $mm^2\,s^{-1}$ for both compounds. In the case of $Ag_5Te_{1.8}Se_{0.2}Cl$ a depression to a minimal value of 0.070 $mm^2\,s^{-1}$ was found at 300.7 K, in close neighborhood to the structural phase transition at 303 K. Compared with Ag_5Te_2Cl, which features a thermal diffusivity of approx. 0.12 $mm^2\,s^{-1}$ for the different polymorphic forms, a significant influence of the substitution is not discernible. The value itself is comparable for instance with that of r. t. diffusivities of insulators [17].

In summary, the results of the thermopower measurements and the thermal diffusivities are comparable to the properties of Ag_5Te_2Cl [11].

The appearance of attractive interactions in $In_4Se_{3-\delta}$ (Peierls-distorted In chain) [4], $Ag_{10}Te_4Br_3$ (Peierls-distorted Te chain) [5] and Ag_5Te_2Cl (d^{10}-d^{10} interaction) [11] has a significant influence on the physical properties. A modulation of the electronic structure can be achieved based on these low-dimensional interactions which do significantly

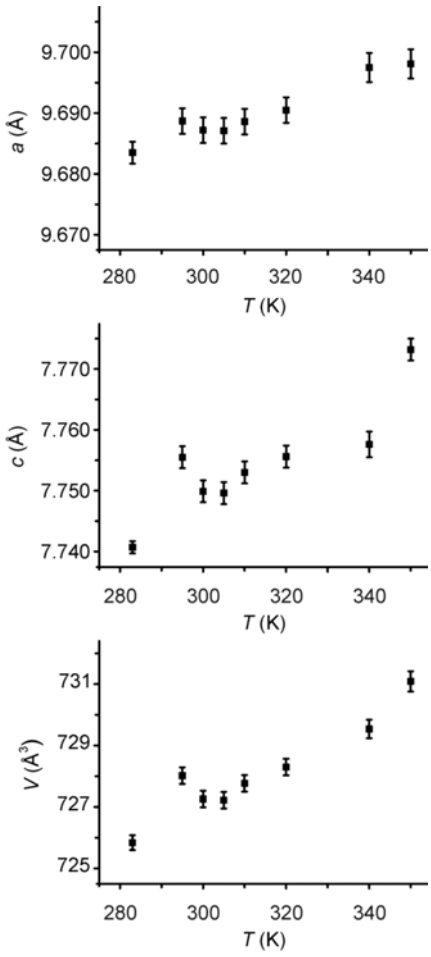

Fig. 4. Temperature-dependent single-crystal X-ray diffraction of $Ag_5Te_{1.6}Se_{0.4}Cl$ in the temperature range 289 – 350 K. The measured lattice parameters of $Ag_5Te_{1.6}Se_{0.4}Cl$ exhibit a negative thermal expansion during heating.

influence the thermopower and the thermal diffusivity of these materials [12, 18]. A strong influence on the electronic structure and the thermopower originating from a Peierls-distorted situation has also been postulated for lead chalcogenides (PbQ with Q = S, Se, Te) under high-pressure conditions [19]. The thermoelectric properties of $Ag_5Te_{1.8}Se_{0.2}Cl$ and $Ag_5Te_{1.6}Se_{0.4}Cl$ are shown in Fig. 3 and the crystallographic parameters of $Ag_5Te_{1.6}Se_{0.4}Cl$ obtained in temperature-dependent experiments in Fig. 4. The expected linear relationship between the temperature and the lattice parameters is present above a temperature of 305 K. Below this temperature an anomaly is observed (negative thermal expansion), which is also assigned to attractive bonding interaction (Fig. 4). This

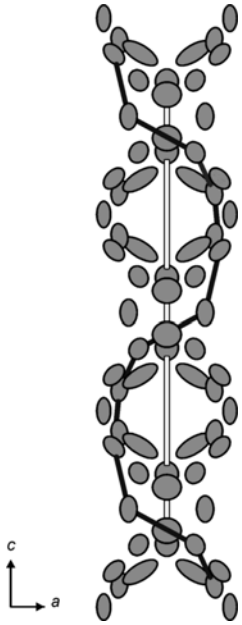

Fig. 5. Two different models for a d^{10}-d^{10} interaction of the silver atoms along the *c* axis in α-Ag_5Te_2Cl-type compounds.

phenomenon was also demonstrated for the ternary counterpart Ag_5Te_2Cl [11]. A negative thermal expansion coefficient was located in supercooled liquid tellurium, which could be related to the accruement of a Peierls-distorted arrangement of Te chains [20]. In the comparable quasi-molten situation of the silver substructure in Ag_5Te_2Cl the formation of attractive interactions can be expected in the same way as for the liquid Te phase [11]. The small standard deviations for each value suggest a limited trend of the lattice parameters (Table 1). Details of the structure determinations and selected crystallographic data are given in Tables 2 to 12. The *c* axis of Ag_5Te_2Cl shows a similar variation. Therefore, two possible mechanisms for the attractive interaction were postulated, an interaction within the helical (black line in Fig. 5) strands and a linear one (white line in Fig. 5) within the strands. For comparison the pattern of α-Ag_5Te_2Cl is shown in Fig. 2. Ag–Ag distances between 2.9 and 3.2 Å cover the usual range of silver compounds featuring d^{10}-d^{10} interactions [21]. In order to substantiate the attractive silver interactions according to the two mechanisms, the Ag–Ag distance was examined in temperature dependent single-crystal structure determinations. The silver arrangement within the strands in α-Ag_5Te_2Cl was determined by a non-harmonic description of the silver displacements and a subsequent detailed probability density function (*pdf*) analysis. The mode positions (suffix *m* added), representing the maxima of

Table 1. Crystallographic data derived from temperature-dependent single-crystal X-ray diffraction experiments of $Ag_5Te_{1.6}Se_{0.4}Cl$ (α-phase, tetragonal, $I4/mcm$) between 283 and 350 K. Each set of lattice parameters is derived from a complete single-crystal data set. The errors of temperature are estimated to be $\pm$0.2 K.

T (K)	*a* (Å)	*c* (Å)	*V* (Å^3)
283	9.6834(6)	7.7407(5)	725.84(8)
295	9.6858(7)	7.7555(6)	726.66(9)
300	9.6872(7)	7.7499(6)	727.26(9)
305	9.6871(7)	7.7496(6)	727.22(9)
310	9.6886(7)	7.7530(6)	727.77(9)
320	9.6905(7)	7.7556(6)	728.30(9)
340	9.6975(8)	7.7576(7)	729.54(11)
350	9.6981(8)	7.7732(6)	731.09(10)

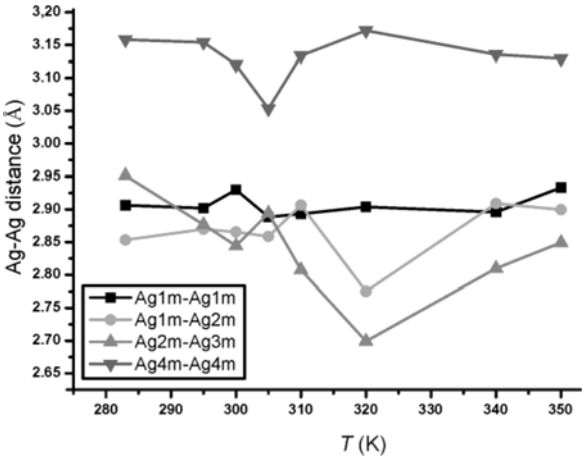

Fig. 6. Distances (Å) between the silver mode positions (suffix m) in α-$Ag_5Te_{1.6}Se_{0.4}Cl$. Ag4m–Ag4m represents the interaction in the linear strand distance between two neighboring silver atoms along the *c* axis. Ag1m–Ag2m and Ag2m–Ag3m are two interactions from the helical-type structure sections (see black line in Fig. 5) within the silver strands, and Ag4m–Ag4m denotes the linear Peierls-like chain arrangement (open line in Fig. 5). The shortest distance between silver ions is *ca.* 2.7 Å.

electron density and therefore the highest probability to find an ion in the respective area, were taken into account to discuss Ag–Ag distances in more detail. The evolution of the Ag_m-Ag_m distances based on these mode positions is shown in Fig. 6 for the temperature range 289 – 350 K. A significant decrease of the Ag–Ag distances is detected for both postulated mechanisms in the helical (Ag1m–Ag2m and Ag2m–Ag3m) and the linear (Ag4m–Ag4m) model. The results are comparable with the effects seen for Ag_5Te_2Cl [11].

The occupancy factors of each silver position are much lower than 1.0, consequently the postulated heli-

Table 2. Crystallographic data for α-$Ag_5Te_{1.6}Se_{0.4}Cl$ at 283, 293 and 295 K.

Temperature, K	283	293	295
Structure type		α-Ag_5Te_2Cl	
Formula weight, g mol^{-1}		812.7	
Crystal system		tetragonal	
Space group		$I4/mcm$	
Unit cell dimensions			
a, Å	9.6834(6)	9.6868(7)	9.6858(7)
c, Å	7.7407(5)	7.7555(6)	7.7555(6)
Volume, Å^3	725.84(8)	728.02(9)	726.66(9)
Z	4	4	4
Density ρ (calculated), g cm^{-3}	7.42	7.41	7.41
Diffractometer		Stoe IPDS II	
Radiation		MoK_α radiation (0.71073 Å), graphite monochromator	
Absorption correction		numerical, X-RED and X-SHAPE [23]	
Absorption coefficent μ, mm^{-1}	21.8	21.8	21.8
F(000), e	1395	1395	1395
θ range, deg	2.97 – 31.98	2.97 – 30.37	2.97 – 31.87
hkl range	−12/14, ±14, −9/11	±13, −10/13, −9/10	−12/14, ±14, −9/11
Total reflections	4151	3321	4156
Independent reflections	314	206	318
R_{int} (all)	0.0441	0.058	0.0501
Refined parameters	80	81	81
R / wR [$I \geq 3\sigma(I)$]	0.0372 / 0.0545	0.0247 / 0.0371	0.0461 / 0.0727
R / wR (all reflections)	0.0428 / 0.0555	0.0295 / 0.0385	0.0531 / 0.0744
Goodness of Fit F^2	3.30	2.51	3.38
$\Delta\rho_{max\,/\,min}$, e Å^{-3}	0.64 / −0.76	0.41 / −0.47	1.39 / −0.71

Table 3. Crystallographic data for α-$Ag_5Te_{1.6}Se_{0.4}Cl$ at 300, 305 and 310 K.

Temperature, K	300	305	310
Structure type		α-Ag_5Te_2Cl	
Formula weight, g mol^{-1}		810.5	
Crystal system		tetragonal	
Space group		$I4/mcm$	
Unit cell dimensions			
a, Å	9.6872(7)	9.6871(7)	9.6886(7)
c, Å	7.7499(6)	7.7496(6)	7.7530(6)
Volume, Å^3	727.26(9)	727.22(9)	727.77(9)
Z	4	4	4
Density ρ (calculated), g cm^{-3}	7.40	7.40	7.40
Diffractometer		Stoe IPDS II	
Radiation		MoK_α radiation (0.71073 Å), graphite monochromator	
Absorption correction		numerical, X-RED and X-SHAPE [23]	
Absorption coefficent μ, mm^{-1}	21.8	21.78	21.8
F(000), e	1395	1395	1395
θ range, deg	2.97 – 31.86	2.97 – 31.86	2.97 – 31.85
hkl range	−12/14, ±14, −9/11	−12/14, ±14, −9/11	−12/14, ±14, −9/11
Total reflections	4165	4168	4179
Independent reflections	332	320	327
R_{int} (all)	0.0662	0.0533	0.048
Refined parameters	81	81	81
R / wR [$I \geq 3\sigma(I)$]	0.0473 / 0.0744	0.0438 / 0.0691	0.0375 / 0.0595
R / wR (all reflections)	0.0544 / 0.0769	0.0517 / 0.0714	0.0439 / 0.0606
Goodness of Fit F^2	3.25	3.32	3.35
$\Delta\rho$max / min, e Å^{-3}	2.02 / −1.01	1.75 / −0.80	0.98 / −0.74

cal and linear silver interactions are not formed within the whole structure. Such an interaction can only be punctual. Therefore, the discontinuous helical silver subunit or Peierls chain in Ag_5Te_2Cl postulated here is rather different compared with the fully translative linear Peierls-distorted In or Te chains in $In_4Se_{3-\delta}$ and $Ag_{10}Te_4Br_3$ [4, 5], respectively. In $Ag_5Te_{2-y}Se_yCl$ the two different structure units, a discontinuous helical silver arrangement or a Peierls chain, can be the two general host units for the formation of attractive

Table 4. Crystallographic data for α-$Ag_5Te_{1.6}Se_{0.4}Cl$ at 320, 340 and 350 K.

Temperature, K	320	340	350
Structure type		α-Ag_5Te_2Cl	
Formula weight, g mol^{-1}		810.5	
Crystal system		tetragonal	
Space group		$I4/mcm$	
Unit cell dimensions			
a, Å	9.6905(7)	9.6975(8)	9.6981(8)
c, Å	7.7556(6)	7.7576(7)	7.7732(6)
Volume, Å^3	728.30(9)	729.54(11)	731.09(10)
Z	4	4	4
Density ρ (calculated), g cm^{-3}	7.39	7.38	7.36
Diffractometer		Stoe IPDS II	
Radiation		MoK_α radiation (0.71073 Å), graphite monochromator	
Absorption correction		numerical, X-RED and X-SHAPE [23]	
Min / max transmission	0.0692 / 0.2013	0.0692 / 0.2121	0.0440 / 0.1876
Absorption coefficent μ, mm^{-1}	21.7	21.7	21.7
$F(000)$, e	1395	1395	1395
θ range, deg	2.97 – 31.85	2.97 – 31.93	2.97 – 31.92
hkl range	−12/14, ±14, −9/11	−12/14, ±14, −9/11	−12/14, ±14, −9/11
Total reflections	4188	4204	4217
Independent reflections	315	318	336
R_{int} (all)	0.049	0.050	0.059
Refined parameters	81	81	81
R / wR [$I \geq 3\sigma(I)$]	0.0401 / 0.0688	0.0387 / 0.0693	0.0392 / 0.0352
R / wR (all reflections)	0.0484 / 0.0705	0.0449 / 0.0712	0.0461 / 0.0362
Goodness of Fit F^2	3.26	2.89	2.90
$\Delta\rho_{max\,/\,min}$, e Å^{-3}	1.44 / −089	0.75 / −0.71	0.97 / −1.03

Table 5. Atomic coordinates, occupancy factors (*sof*) and isotropic displacement parameters U_{eq} (Å^2) of α-$Ag_5Te_{1.6}Se_{0.4}Cl$ at 283 K. Standard deviations are given in parentheses. The mode positions (*mode pos.*, suffix *m*) were calculated from the PDF and represent the maxima of electron density for the position concerned. It represents the highest probability to find a silver ion in the respective area.

Atom	Wyckoff	x	y	z	*sof*	U_{eq}
Te1	8*h*	0.16293(6)	0.33707(6)	1/2	0.8	0.0539(2)
Se1	8*h*	0.16293(6)	0.33707(6)	1/2	0.2	0.0539(2)
Cl2	4*a*	0	0	1/4	1	0.0404(5)
Ag1	16*k*	0.2977(10)	0.5756(8)	1/2	0.325(8)	0.092(3)
Ag2	32*m*	−0.0669(8)	0.2635(10)	0.3264(11)	0.290(6)	0.117(3)
Ag3	16*l*	0.1386(12)	0.3614(12)	0.150(2)	0.167(12)	0.142(6)
Ag4	16*l*	0.074(1)	0.426(1)	0.2003(18)	0.178(19)	0.175(4)
Ag1m	*mode pos.*	0.3000	0.5710	0.5000		
Ag2m	*mode pos.*	−0.0903	0.2603	0.3499		
Ag3m	*mode pos.*	0.1327	0.3673	0.1271		
Ag4m	*mode pos.*	0.0490	0.4510	0.2040		

Table 6. Atomic coordinates, occupancy factors (*sof*) and isotropic displacement parameters U_{eq} (Å^2) of α-$Ag_5Te_{1.6}Se_{0.4}Cl$ at 295 K. Standard deviations are given in parentheses. The mode positions (*mode pos.*, suffix *m*) were calculated from the PDF and represent the maxima of electron density for the position concerned. It represents the highest probability to find a silver ion in the respective area.

Atom	Wyckoff	x	y	z	*sof*	U_{eq}
Te1	8*h*	0.16304(7)	0.33696(7)	1/2	0.8	0.0543(3)
Se1	8*h*	0.16304(7)	0.33696(7)	1/2	0.2	0.0543(3)
Cl2	4*a*	0	0	1/4	1	0.0404(6)
Ag1	16*k*	0.2967(13)	0.5714(10)	1/2	0.309(10)	0.089(3)
Ag2	32*m*	−0.0680(8)	0.2642(11)	0.3217(11)	0.277(8)	0.114(4)
Ag3	16*l*	0.1387(17)	0.3613(17)	0.118(3)	0.192(17)	0.161(10)
Ag4	16*l*	0.0758(14)	0.4242(14)	0.189(2)	0.20(3)	0.189(5)
Ag1m	*mode pos.*	0.3010	0.5727	0.5000		
Ag2m	*mode pos.*	−0.0886	0.2618	0.3454		
Ag3m	*mode pos.*	0.1324	0.3676	0.1355		
Ag4m	*mode pos.*	0.0509	0.4491	0.2036		

interactions. The most probable unit, taking into account the occupancy factors between 0.36 and 0.16 for each silver position in $Ag_5Te_{1.6}Se_{0.4}Cl$, is that with the alignment of simple ion pairs within the helical pathway (Tables 5 – 12). After a detailed analysis of the silver distribution, the smallest Ag_m-Ag_m distance of approx. 2.7 Å and therefore the most probable domain of interactions were found in the helical subunit.

Analogous to the evolution of attractive interactions within the silver substructure in $Ag_5Te_{1.6}Se_{0.4}Cl$,

Atom	Wyckoff	x	y	z	sof	U_{eq}
Te1	8*h*	0.16272(7)	0.33728(7)	1/2	0.8	0.0550(3)
Se1	8*h*	0.16272(7)	0.33728(7)	1/2	0.2	0.0550(3)
Cl2	4*a*	0	0	1/4	1	0.0429(7)
Ag1	16*k*	0.2985(14)	0.5713(11)	1/2	0.309(11)	0.090(3)
Ag2	32*m*	−0.0685(9)	0.2648(13)	0.3206(18)	0.273(9)	0.116(4)
Ag3	16*l*	0.1364(19)	0.3636(19)	0.118(3)	0.22(2)	0.176(11)
Ag4	16*l*	0.0764(12)	0.4236(12)	0.184(2)	0.17(3)	0.201(5)
Ag1m	*mode pos.*	0.2999	0.5731	0.5000		
Ag2m	*mode pos.*	−0.0881	0.2605	0.3452		
Ag3m	*mode pos.*	0.1307	0.3693	0.1417		
Ag4m	*mode pos.*	0.0490	0.4510	0.2013		

Table 7. Atomic coordinates, occupancy factors (*sof*) and isotropic displacement parameters U_{eq} (Å^2) of α-$Ag_5Te_{1.6}Se_{0.4}Cl$ at 300 K. Standard deviations are given in parentheses. The mode positions (*mode pos.*, suffix *m*) were calculated from the PDF and represent the maxima of electron density for the position concerned. It represents the highest probability to find a silver ion in the respective area.

Atom	Wyckoff	x	y	z	sof	U_{eq}
Te1	8*h*	0.16265(7)	0.33735(7)	1/2	0.8	0.0546(3)
Se1	8*h*	0.16265(7)	0.33735(7)	1/2	0.2	0.0546(3)
Cl2	4*a*	0	0	1/4	1	0.0428(7)
Ag1	16*k*	0.3001(12)	0.5690(9)	1/2	0.312(9)	0.089(3)
Ag2	32*m*	−0.0701(9)	0.2676(13)	0.3191(17)	0.286(8)	0.118(4)
Ag3	16*l*	0.133(2)	0.367(2)	0.113(3)	0.201(18)	0.168(8)
Ag4	16*l*	0.0735(11)	0.4265(11)	0.181(2)	0.16(3)	0.197(5)
Ag1m	*mode pos.*	0.3007	0.5688	0.5000		
Ag2m	*mode pos.*	−0.0907	0.2642	0.3464		
Ag3m	*mode pos.*	0.1332	0.3668	0.1352		
Ag4m	*mode pos.*	0.0507	0.4493	0.1970		

Table 8. Atomic coordinates, occupancy factors (*sof*) and isotropic displacement parameters U_{eq} (Å^2) of α-$Ag_5Te_{1.6}Se_{0.4}Cl$ at 305 K. Standard deviations are given in parentheses. The mode positions (*mode pos.*, suffix *m*) were calculated from the PDF and represent the maxima of electron density for the position concerned. It represents the highest probability to find a silver ion in the respective area.

Atom	Wyckoff	x	y	z	sof	U_{eq}
Te1	8*h*	0.16243(6)	0.33757(6)	1/2	0.8	0.0546(3)
Se1	8*h*	0.16243(6)	0.33757(6)	1/2	0.2	0.0546(3)
Cl2	4*a*	0	0	1/4	1	0.0448(6)
Ag1	16*k*	0.2964(13)	0.5718(9)	1/2	0.327(10)	0.098(4)
Ag2	32*m*	−0.0695(10)	0.2639(12)	0.3236(16)	0.275(8)	0.117(4)
Ag3	16*l*	0.1390(19)	0.3610(19)	0.136(3)	0.194(18)	0.148(8)
Ag4	16*l*	0.0749(12)	0.4251(12)	0.1897(16)	0.18(3)	0.196(5)
Ag1m	*mode pos.*	0.2998	0.5725	0.5000		
Ag2m	*mode pos.*	−0.0894	0.2594	0.3463		
Ag3m	*mode pos.*	0.1305	0.3695	0.1401		
Ag4m	*mode pos.*	0.0483	0.4517	0.2016		

Table 9. Atomic coordinates, occupancy factors (*sof*) and isotropic displacement parameters U_{eq} (Å^2) of α-$Ag_5Te_{1.6}Se_{0.4}Cl$ at 310 K. Standard deviations are given in parentheses. The mode positions (*mode pos.*, suffix *m*) were calculated from the PDF and represent the maxima of electron density for the position concerned. It represents the highest probability to find a silver ion in the respective area.

Atom	Wyckoff	x	y	z	sof	U_{eq}
Te1	8*h*	0.16223(6)	0.33777(6)	1/2	0.8	0.0561(3)
Se1	8*h*	0.16223(6)	0.33777(6)	1/2	0.2	0.0561(3)
Cl2	4*a*	0	0	1/4	1	0.0467(7)
Ag1	16*k*	0.293(2)	0.5716(11)	1/2	0.355(14)	0.107(5)
Ag2	32*m*	−0.0711(10)	0.2655(13)	0.3167(18)	0.269(9)	0.114(4)
Ag3	16*l*	0.1369(19)	0.3631(19)	0.111(4)	0.20(2)	0.159(10)
Ag4	16*l*	0.0772(14)	0.4228(14)	0.1777(19)	0.16(3)	0.213(4)
Ag1m	*mode pos.*	0.3007	0.5720	0.5000		
Ag2m	*mode pos.*	−0.0879	0.2627	0.3435		
Ag3m	*mode pos.*	0.1330	0.3670	0.1368		
Ag4m	*mode pos.*	0.0510	0.4490	0.2045		

Table 10. Atomic coordinates, occupancy factors (*sof*) and isotropic displacement parameters U_{eq} (Å^2) of α-$Ag_5Te_{1.6}Se_{0.4}Cl$ at 320 K. Standard deviations are given in parentheses. The mode positions (*mode pos.*, suffix *m*) were calculated from the PDF and represent the maxima of electron density for the position concerned. It represents the highest probability to find a silver ion in the respective area.

along the helical silver subunit the Ag2m–Ag3m distance drops significantly with increasing temperature to a minimum value of 2.7 Å at 320 K. Around this temperature the thermopower stays on a minimum plateau (Fig. 3). Therefore, the origin of the thermopower behavior is most likely to be found in the helical arrangement based on distance considerations. This finding is in contrast to $Ag_{10}Te_4Br_3$ and $In_4Se_{3-\delta}$ where linear Peierls-distorted chains are the origin of interactions. Furthermore, for ternary Ag_5Te_2Cl a DFT (GGA) calculation of the isolated silver structure shows the influence of close Ag^+-Ag^+ contacts.

Atom	Wyckoff	*x*	*y*	*z*	*sof*	U_{eq}
Te1	8*h*	0.16219(7)	0.33781(7)	1/2	0.8	0.0556(2)
Se1	8*h*	0.16219(7)	0.33781(7)	1/2	0.2	0.0556(2)
Cl2	4*a*	0	0	1/4	1	0.0462(6)
Ag1	16*k*	0.2951(16)	0.5730(10)	1/2	0.303(12)	0.090(3)
Ag2	32*m*	−0.0697(9)	0.2622(12)	0.3241(15)	0.282(8)	0.119(4)
Ag3	16*l*	0.1429(15)	0.3571(15)	0.134(3)	0.20(2)	0.174(10)
Ag4	16*l*	0.0808(14)	0.4192(14)	0.1888(18)	0.18(3)	0.226(6)
Ag1m	*mode pos.*	0.3011	0.5709	0.5000		
Ag2m	*mode pos.*	−0.0881	0.2603	0.3412		
Ag3m	*mode pos.*	0.1326	0.3674	0.1484		
Ag4m	*mode pos.*	0.0535	0.4465	0.2021		

Table 11. Atomic coordinates, occupancy factors (*sof*) and isotropic displacement parameters U_{eq} (Å^2) of α-$Ag_5Te_{1.6}Se_{0.4}Cl$ at 340 K. Standard deviations are given in parentheses. The mode positions (*mode pos.*, suffix *m*) were calculated from the PDF and represent the maxima of electron density for the position concerned. It represents the highest probability to find a silver ion in the respective area.

Atom	Wyckoff	*x*	*y*	*z*	*sof*	U_{eq}
Te1	8*h*	0.16182(6)	0.33819(6)	1/2	0.8	0.0569(3)
Se1	8*h*	0.16182(6)	0.33819(6)	1/2	0.2	0.0569(3)
Cl2	4*a*	0	0	1/4	1	0.0497(6)
Ag1	16*k*	0.289(2)	0.5747(11)	1/2	0.356(11)	0.123(5)
Ag2	32*m*	−0.0732(14)	0.2615(16)	0.3160(18)	0.258(8)	0.125(5)
Ag3	16*l*	0.134(2)	0.366(2)	0.124(4)	0.19(2)	0.144(8)
Ag4	16*l*	0.0789(17)	0.4202(17)	0.195(2)	0.19(3)	0.216(6)
Ag1m	*mode pos.*	0.3007	0.5688	0.5000		
Ag2m	*mode pos.*	−0.0907	0.2642	0.3464		
Ag3m	*mode pos.*	0.1332	0.3668	0.1352		
Ag4m	*mode pos.*	0.0507	0.4493	0.1970		

Table 12. Atomic coordinates, occupancy factors (*sof*) and isotropic displacement parameters U_{eq} (Å^2) of α-$Ag_5Te_{1.6}Se_{0.4}Cl$ at 350 K. Standard deviations are given in parentheses. The mode positions (*mode pos.*, suffix *m*) were calculated from the PDF and represent the maxima of electron density for the position concerned. It represents the highest probability to find a silver ion in the respective area.

Total energy calculations clearly indicate a distortion of isolated Ag^+ ions toward the formation of $(Ag^+)_2$ pairs [11]. Compounds like $Ag_5Te_{2-y}Se_yCl$ are the second, but also isostructural examples of silver ion-conducting systems with a high silver mobility and a formation of d^{10}-d^{10} interactions.

Conclusion

In $Ag_5Te_{1.6}Se_{0.4}Cl$ attractive d^{10}-d^{10} interactions have been identified at higher temperatures close after the β-α phase transition, resulting in significant effects on the thermopower and on the crystallographic parameters. It is highly probable that silver ion pair formation along a helical arrangement of silver sites is the origin of these modulations. The minimum value of the thermopower is reached at the point of the strongest interactions near the β-α phase transition, and it starts to rise upon further heating. The situation is more pronounced in the case of $Ag_5Te_{1.8}Se_{0.2}Cl$ where the lower grade of substitution has a stronger influence on the property modulations and the thermopower. This feature is caused by a decreasing contribution of d^{10}-d^{10} interactions in the silver substructure. Consistent with a recent observation, that a Peierls-distorted arrangement of either anionic or cationic chains can cause a pronounced modulation of the electric and thermoelectric properties, the present study substantiates the possibility to use weak attractive interactions, such as d^{10}-d^{10} contacts, to initiate substantial variations of physical properties.

Experimental Section

Synthesis

$Ag_5Te_{1.8}Se_{0.2}Cl$ and $Ag_5Te_{1.6}Se_{0.4}Cl$ were prepared from stoichiometric mixtures of Ag (Heraeus, 99.99 %), Se (Chempur, 99.999 %), Te (Chempur, 99.9999 %), and AgCl (Alfa Aesar, 99.9 %). All starting materials were used without further purification [13]. The mixtures were sealed in evacuated silica ampoules, heated to 1173 K, held at this temperature for 3 h and quenched in an ice bath. After a homogenization step the mixtures were annealed at 613 K for 7 d for each run. The homogenization and annealing process was repeated twice in order to achieve phase purity of the samples. After homogenization steps the purity was checked by powder X-ray diffraction experiments. The compounds are light- and moisture-stable and can be stored and handled in air for several months.

Powder X-ray diffraction

Phase analyses were performed by powder X-ray diffraction measurements. The sample was characterized *via* Guinier powder patterns using Cu$K_{\alpha 1}$ radiation and α-quartz (a = 4.913 Å and c = 5.405 Å) as an internal standard at 298 K. The Guinier camera was operated with image plate technology, and read-out was achieved with a Fuji-film/BAS-1800 image plate system. The lattice parameters were re-

fined from the powder data for phase-pure $Ag_5Te_{1.8}Se_{0.2}Cl$ to a = 13.809(5) Å, b = 7.629(4) Å, c = 13.588(6) Å, β = 90.89(2) and V = 1431.2(14) Å^3 by fitting the metrics of the β-Ag_5Te_2Cl structure type. For phase-pure $Ag_5Te_{1.6}Se_{0.4}Cl$ the parameters are a = 9.703(3) Å, c = 7.760(3) Å and V = 730.6(6) Å^3 featuring the α-Ag_5Te_2Cl structure type.

Single-crystal X-ray diffraction

Data of $Ag_5Te_{1.6}Se_{0.4}Cl$ were collected at 283, 295, 298, 300, 305, 310, 320, 340, and 350 K on a Stoe IPDS II diffractometer with MoK_α radiation (λ = 0.71073 Å). Temperature-dependent measurements were carried out using a Cryostream plus system (Oxford) with an accuracy of the absolute temperature of ±0.5 K and a temperature stability of ±0.1 K during the data collection. A numerical absorption correction [22] was performed independently for each data set based on an optimized crystal shape derived from the symmetry-equivalent reflections. The structure refinements [23] were based on the previously reported structure models for the β- and α-Ag_5Te_2Cl phase using non-harmonic displacement parameters up to the third order for the description of the silver ion distribution. All silver mode positions are derived from the maxima of electron density and are used for a discussion of the average silver ion distances within the silver substructure. A detailed procedure for the structure refinement of compounds featuring high ion mobility in the solid state is given elsewhere [14, 24].

Further details of the crystal structure investigation may be obtained from Fachinformationszentrum Karlsruhe, 76344 Eggenstein-Leopoldshafen, Germany (fax: +49-7247-808-666; e-mail: crysdata@fiz-karlsruhe.de, http://www.fizinformationsdienste.de/en/DB/icsd/depot_anforderung.html) on quoting the deposition numbers
CSD-423325 (283 K, α-$Ag_5Te_{1.6}Se_{0.4}Cl$),
CSD-423326 (293 K, α-$Ag_5Te_{1.6}Se_{0.4}Cl$),
CSD-423327 (295 K, α-$Ag_5Te_{1.6}Se_{0.4}Cl$),
CSD-423328 (300 K, α-$Ag_5Te_{1.6}Se_{0.4}Cl$),
CSD-423329 (305 K, α-$Ag_5Te_{1.6}Se_{0.4}Cl$),
CSD-423330 (310 K, α-$Ag_5Te_{1.6}Se_{0.4}Cl$),
CSD-423331 (320 K, α-$Ag_5Te_{1.6}Se_{0.4}Cl$),
CSD-423332 (340 K, α-$Ag_5Te_{1.6}Se_{0.4}Cl$) and
CSD-423333 (350 K, α-$Ag_5Te_{1.6}Se_{0.4}Cl$).

Thermal diffusivity

Powdered samples of $Ag_5Te_{1.8}Se_{0.2}Cl$ and $Ag_5Te_{1.6}Se_{0.4}Cl$ were pressed to pellets of 6 mm in diameter and *ca.* 2 mm thickness reaching a value of > 98 % of the theoretical X-ray density. Independent measurements were performed for a pellet covering the temperature range of 300 to 500 K. The thermal diffusivity was measured by a commercial Netzsch Laser Microflash apparatus in a SiC sample holder under Ar atmosphere. The average values of five independent measurements were calculated for each data point in the temperature range of 300 to 500 K. The thermal diffusivity was derived from the raw data using the Proteus software package.

Thermopower

$Ag_5Te_{1.8}Se_{0.2}Cl$ and $Ag_5Te_{1.6}Se_{0.4}Cl$ pellets used for the measurements of thermal diffusivity (6 mm diameter and *ca.* 2 mm thickness) were transferred to a homemade thermopower machine, and data were determined in the temperature range of 300 – 500 K. The thermopower measurements were carried out using a dynamic method (constant heating during the measurement, detection of the cell voltage *versus* time; accuracy of the thermopower within ±1 %), suitable for high-resistivity samples as well as metals featuring a thermopower lower than 10 μV K^{-1}. Details of the measuring cell and the measurement technique are described elsewhere [25].

EDX analyses

Semi-quantitative analysis of the sample was performed using a Leica 420i scanning electron microscope (Zeiss) fitted with an electron dispersive detector unit (Oxford). Silver, selenium, HgTe (Te), KBr (Br), KCl (Cl), and FeS_2 (S) were used as standards for calibration. A voltage of 20 kV was applied to the samples. The postulated composition was substantiated within the standard deviations of the method.

Differential scanning calorimetry (DSC)

DSC measurement was performed with a Netzsch differential scanning calorimeter DSC 204 at heating and cooling rates of 10 K min^{-1} in the temperature range between 150 and 625 K. Mercury, indium, tin, bismuth, zinc, and cesium chloride were used for temperature calibration. All samples were measured under a constant nitrogen flow of 50 mL min^{-1} in sealed aluminum crucibles.

Acknowledgement

T. N. thanks the University of Bordeaux for the invitation as a Guest Professor and for the possibility to perform parts of this work. This work is financed by the DFG (NI 1095/3-1).

[1] C. J. Vineis, A. Shakouri, A. Majumdar, M. G. Kanatzidis, *Adv. Mater.* **2010**, *22*, 3970.
[2] W. Zheng, J. Zhang , B. Zhu, R. Blume, Y. Zhang, K. Schlichte, R. Schlögl, F. Schüth, D. S. Su, *Chem. Sus. Chem.* **2010**, *3*, 209.
[3] J. R. Sootsman, D. Y. Chung, M. G. Kanatzidis, *Angew.*

Chem. **2009**, *121*, 8768; *Angew. Chem. Int. Ed.* **2009**, *48*, 8616.
[4] J.-S. Rhyee, K. H. Lee, S. M. Lee, E. Cho, S. I. Kim, E. Lee, Y. S. Kwon, J. H. Shim, G. Kotliar, *Nature* **2009**, *459*, 965.
[5] T. Nilges, S. Lange, M. Bawohl, J. M. Deckwart, M. Janssen, H.-D. Wiemhöfer, R. Decourt, B. Chevalier, J. Vannahme, H. Eckert, R. Weihrich, *Nat. Mater.* **2009**, *8*, 101.
[6] J. Janek, *Nat. Mater.* **2009**, *8*, 88.
[7] D. Pitzschke, J. Curda, G. Cakmak, M. Jansen, *Z. Anorg. Allg. Chem.* **2008**, *634*, 1071.
[8] D. Pitzschke, J. Curda, G. Cakmak, M. Jansen, *Z. Anorg. Allg. Chem.* **2008**, *634*, 1907.
[9] D. Pitzschke, J. Curda, M. Jansen, *Z. Anorg. Allg. Chem.* **2009**, *635*, 926.
[10] H. Kleinke, *Molecules* **2009**, *14*, 3115.
[11] T. Nilges, O. Osters, M. Bawohl, J.-L. Bobet, B. Chevalier, R. Decourt, R. Weihrich, *Chem. Mater.* **2010**, *22*, 2946.
[12] N. Eckstein, T. Nilges, R. Decourt, J.-L. Bobet, B. Chevalier, *J. Solid State Chem.* **2011**, *184*, 778.
[13] J. Messel, T. Nilges, *Z. Naturforsch.* **2008**, *63b*, 1077.
[14] T. Nilges, S. Nilges, A. Pfitzner, T. Doert, P. Böttcher, *Chem. Mater.* **2004**, *16*, 806.
[15] T. Nilges, C. Dreher, A. Heizinger, *Solid State Sci.* **2005**, *7*, 79.
[16] M. Bawohl, T. Nilges, *Z. Naturforsch.* **2008**, *63b*, 1083.
[17] J. Moorikawa, T. Hashimoto, *Polymer* **1997**, *38*, 5397.
[18] T. Nilges, M. Bawohl, O. Osters, S. Lange, J. Messel, *Z. Phys. Chem.* **2010**, *224*, 1.
[19] S. V. Ovsyannikov, V. V. Shchennikov, S. V. Popova, A. Y. Derevskov, *Phys. Stat. Sol. (b)*, **2003**, *235*, 521.
[20] G. Zhao, Y. N. Wu, *Phys. Rev. B* **2009**, *79*, 184203.
[21] M. Jansen, *Angew. Chem*. **1987**, *99*, 1136; *Angew. Chem., Int. Ed. Engl.* **1987**, *26*, 1098.
[22] a) X-RED32 (version 1.10), Data Reduction Program, Stoe & Cie GmbH, Darmstadt (Germany), **2004**; b) X-SHAPE (version 2.05), Crystal Optimization for Numerical Absorption Correction, Stoe & Cie GmbH, Darmstadt (Germany), **2004**.
[23] V. Petříček, M. Dušek, L. Palatinus, JANA2006. The Crystallographic Computing System; Institute of Physics, University of Prague, Prague (Czech Republic) **2006**.
[24] S. Lange, M. Bawohl, T. Nilges, *Inorg. Chem.* **2008**, *47*, 2625.
[25] P. Dordor, E. Marquestaut, G. Villeneuve, *Rev. Phys. Appl.* **1980**, *15*, 1607.